Dynamic Phase Transitions in Cell Spreading

Hans-Günther Döbereiner,* Benjamin Dubin-Thaler, Grégory Giannone, Harry S. Xenias, and Michael P. Sheetz
Department of Biological Sciences, Columbia University, New York, New York 10027, USA
(Received 21 April 2004; published 2 September 2004)

We monitored isotropic spreading of mouse embryonic fibroblasts on fibronectin-coated substrates. Cell adhesion area versus time was measured via total internal reflection fluorescence microscopy. Spreading proceeds in well-defined phases. We found a power-law area growth with distinct exponents in three sequential phases, which we denote as basal, continuous, and contractile spreading. High resolution differential interference contrast microscopy was used to characterize local membrane dynamics at the spreading front. Fourier power spectra of membrane velocity reveal the sudden development of periodic membrane retractions at the transition from continuous to contractile spreading. We propose that the classification of cell spreading into phases with distinct functional characteristics and protein activity serves as a paradigm for a general program of a phase classification of cellular phenotype.

DOI: 10.1103/PhysRevLett.93.108105 PACS numbers: 87.17.–d, 05.45.–a

Cells need to be mobile in order to perform many critical biological functions. The reorganization of extracellular matrix in wound healing, the positioning of nerve cells, or the engulfment of bacteria in the immune reaction of white blood cells are particular examples [1]. Accomplishing this variety of functions requires a diverse set of mechanisms and proteins. Most components of the molecular machinery of actin-based motility have been identified [2–4]. It has been possible to perform experiments with reconstituted systems of Listeria propulsion [5,6] for which detailed elastic models have been developed [7]. Whole cell spreading on matrix-coated surfaces provides a simplified system of analyzing motile behavior. A substantial amount of experimental and theoretical work has been done along these lines [8–11]. However, only quite recently, quantitative experiments of cell spreading and subsequent migration could be performed with high spatial and temporal resolution [12,13]. We found that there are well-defined and distinct states of spreading. It is the goal of this work to show that these states can indeed be considered phases of motility by demonstrating the existence of dynamic phase transitions between them.

Spreading cells extend a 200 nm thick sheet called the lamellipodium from the cell body onto the substrate; see Fig. 1. This process is driven by actin polymerization at the leading membrane edge, the precise mechanism of which is still under debate [14,15]. The meshwork of actin fibers is cross-linked by various proteins. The molecular motor myosin II enables the meshwork to contract by moving along actin fibers relative to other cytoskeletal elements. Thus, the lamellipodium is an active gel enclosed in a flat membrane bag adhering to the substrate. The physics of active gels has recently attracted a lot of attention. Rheological experiments of simple mixtures of purified actin and myosin solutions [16] and quite general theoretical modeling [17,18] have been carried out. These models indicate dynamic phase transitions involving extended and contracted actin density states as a function of myosin-actin coupling strength [17]. We will show that our cellular system exhibits similar transitions which express themselves prominently in the dynamics of the leading membrane edge.

Mouse embryonic fibroblasts (MEF) were allowed to adhere to fibronectin-coated glass slides and observed with either total internal reflection fluorescence (TIRF) or differential interference contrast (DIC) microscopy. Fibronectin is an extracellular matrix protein which is linked to the cytoskeleton via integrin receptors within the membrane. TIRF studies were performed at a moderate spatial and temporal resolution to capture overall spreading characteristics of the whole cell. Multiple cells could be studied simultaneously. High resolution DIC was used to characterize local membrane dynamics. Details of the methods may be found in our earlier work [12,13].

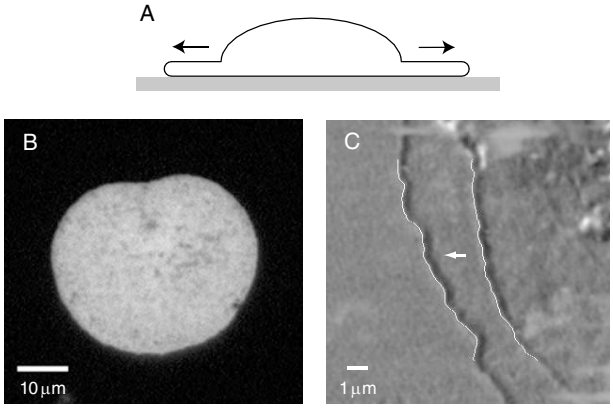

FIG. 1. (a) During cell spreading, a thin lamellipodial sheet extends from the cell body onto the substrate. (b) Total internal reflection fluorescence micrograph of a spreading cell. The bright region corresponds to the area adhered to the substrate. (c) Two overlayed snapshots of the leading membrane edge of a lamellipodium moving from right to left are shown in differential interference contrast. The edge position is marked with a white contour overlay.

Membrane adhesion area A during spreading was best monitored using TIRF. We found distinct classes of angular isotropic and anisotropic spreading cells [12]. More than 70% of all cells exhibited isotropic spreading when grown in culture medium lacking serum, compared to only 20% with normal serum levels (10% calf serum). In the following, we limit ourselves to the isotropic class of serum deprived cells that lack filopodia. Close inspection of double logarithmic plots of adhesion area A over time reveals three phases with distinctly different power-law growth, as seen in Fig. 2. We define area growth exponents a_i via

$$A(t) \sim t^{a_i}, \tag{1}$$

where i denotes the subsequent phases. Initially, there is a basal phase where cells test the suitability of the substrate to adhere and area growth is mimimal. We find $a_1 = 0.4 \pm 0.2$. Then follows a phase of fast continuous spreading, which is characterized by $a_2 = 1.6 \pm 0.9$. Finally, the cell slows down again exhibiting a sublinear area growth with $a_3 = 0.3 \pm 0.2$. We will see below that the latter phase is characterized by periodic local contractions of the cell [13]. Nevertheless, the mean area growth leads to an effective power-law behavior also in this phase. Histograms of exponents a_i for the three phases are shown in Fig. 3. There is a clear distinction of fast area growth in the continuous spreading phase with a rather broad distribution of the exponent a_2. However, we find two narrow clusters when discriminating with respect to the relative area growth, A_2/A_1, during that phase, where A_i denotes the adhesion area at the transition from phase i to $i + 1$. Small ($A_2/A_1 < 5$) or large ($A_2/A_1 > 5$) area increases correspond to small ($a_2 = 0.9 \pm 0.2$) or large ($a_2 = 1.6 \pm 0.2$) exponents, respectively. In addition, there were two single cells with even larger exponents a_2, which we excluded from the cluster average.

The transition from continuous to contractile spreading was further monitored using high resolution DIC. A suitable isotropically spreading cell was chosen and a well resolvable and approximately straight membrane segment was selected for prolonged observation; see Fig. 1(c). Time-lapse sequences were obtained at video rate. Movies were digitized at $1/\Delta t = 3$ Hz. Individual frames are counted using an index n. The cell edge is determined with a custom C program by a local contour algorithm [19,20] allowing nanometer accuracy. We obtain a subpixel resolution of 15 nm for relative displacements, which translates into a minimal detectable velocity of 45 nm/s between frames. Further analysis proceeds using a Cartesian coordinate system where the average membrane orientation is taken as the fixed y axis. Points on the membrane are then labeled by their y coordinates y_j, and the membrane velocity $v_j(n) = \Delta x_j(n)/\Delta t$ is measured along the x axis which is normal to the average membrane orientation.

A typical velocity map along the contour over time is shown in Fig. 4. We find that a region of continuous, uninterrupted spreading (red shadows) precedes a se-

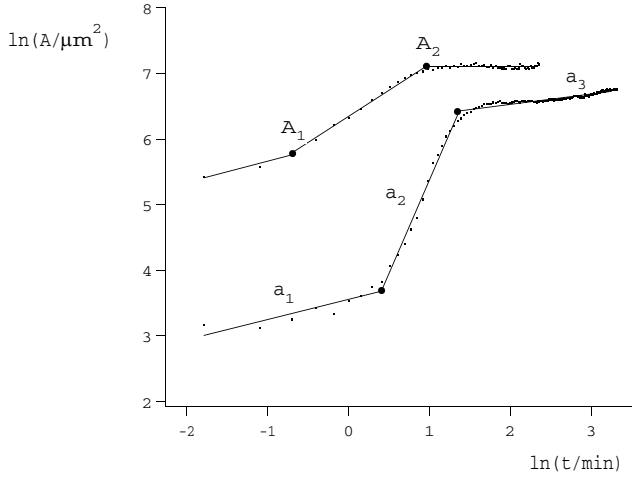

FIG. 2. Adhesion area in isotropically spreading fibroblasts grows with a power law in time. Different but constant exponents a_i in the various phases of spreading are evident in a double logarithmic plot. Exponents have been determined by fitting a piecewise linear function to the data; see Fig. 3. Adhesion areas A_i at the transition points are indicated.

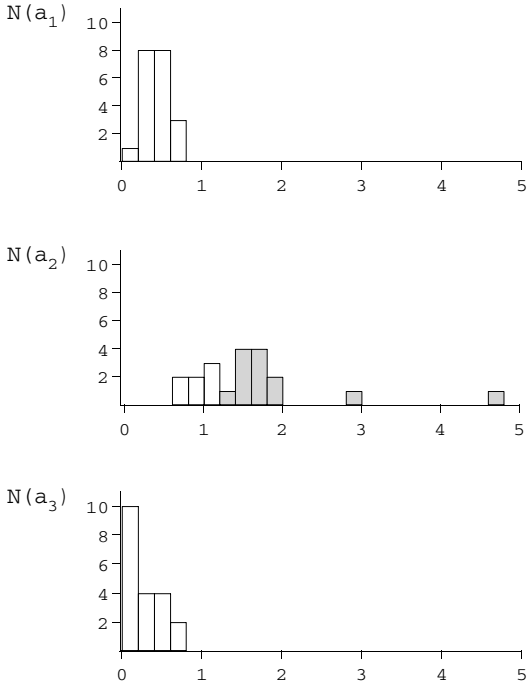

FIG. 3. Histograms of area growth exponents as obtained from the slopes of double logarithmic plots of adhesion area versus time, such as the ones shown in Fig. 2. We have analyzed 20 cells in total. The middle (continuous spreading) phase exhibits clustering corresponding to small (open bars) and large (solid bars) area growth during that phase.

quence of periodic membrane retraction events (blue stripes). These two different states of membrane dynamics correspond to the continuous spreading and contractile phase of the lamellipodium, found above. The two phases can be clearly distinguished using the discrete Fourier transformation $v(s)$ of the velocity map $v(n)$ defined as

$$v_j(s) = \frac{1}{N}\sum_{n=1}^{N} v_j(n)\exp\left(2\pi i\frac{(n-1)(s-1)}{N}\right), \quad (2)$$

where N is the total number of frames. Averages are taken over spatial regions of interest. The continuous spreading phase is characterized by a strong boundary maximum of the spectrum $|v_j(s)|$ at $s = 1$; see Fig. 5(a). In contrast, in the contractile phase the spectrum develops a pronounced peak at $s = s_{\max}$ (see Fig. 5(b)), which signals oscillatory behavior with a period

$$T = \Delta t\frac{N}{s_{\max} - 1}. \quad (3)$$

Thus, the peak position of the power spectrum serves as an excellent phase indicator. We calculate the spectrum inside a small time window—with a width on the order of the repeat time—and sweep across the phase boundary. Indeed, there is a well-defined transition between the two phases, as seen in Fig. 5(c). However, the periodic contractions do not take place simultaneously along the leading edge; see Fig. 4. In fact, there are lateral waves of maximum contraction velocity running in both directions. These waves have a speed on the order of 200 nm/s. Moreover, there are sharp phase shifts of the periodic contractions up to half a period; see encircled region in Fig. 4.

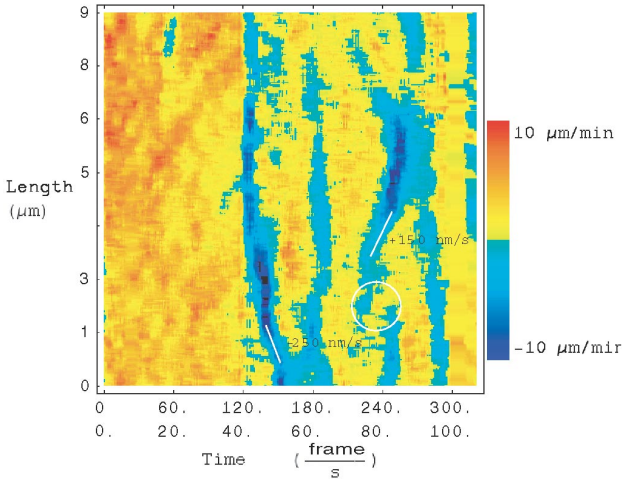

FIG. 4 (color). Normal velocity map of the particular membrane segment marked in Fig. 1(b) as a function of time. Note the two qualitatively different sections before and after time $t = 40$ s corresponding to a continuous and a periodically contractile spreading phase, respectively. The period of the latter is $T = 17 \pm 4$ s. The speeds of lateral waves of maximum contraction velocity are indicated. The encircled region marks a phase shift of a contraction.

In summary, we have seen clear signatures of two different dynamic phase transitions in the spreading behavior of MEF cells. These are (i) the initiation of fast continuous spreading after a period of basal activity, and, subsequently, (ii) the start of periodic membrane retractions. How are these transitions controlled by the cell? The onset of continuous spreading is characterized by an increase in the actin polymerization velocity at the leading edge of the lamellipodium pushing the membrane forward. Increased polymerization is triggered by favorable contact with the extracelluar matrix. We found that the time from contact until initiation of spreading decreases with fibronectin density [12], suggesting an integration of a chemical signal from integrin receptors binding to fibronectin. It follows from the histogram of area growth exponent a_2 that the radial edge velocity ($dR/dt \sim t^{a_2/2-1}$) is typically maximal at the onset of spreading and diminishes during the continuous spreading phase. Indeed, we have $(a_2/2 - 1) < 0$, except for two cells.

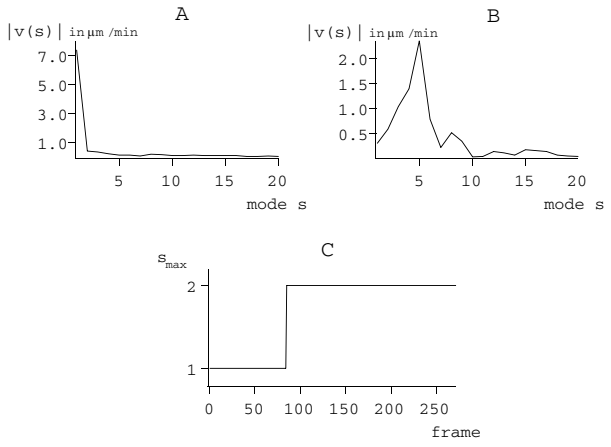

FIG. 5. Fourier spectrum [see Eq. (2)] of the velocity map in Fig. 4 for the two different spreading phases below [(a), $N = 120$] and above [(b) $N = 200$] frame number $n = 120$. The spectrum is spatially averaged over 70 points between position 2.0 and 3.8 μm along the contour. The transition between continuous and contractile spreading is characterized by a sharp shift in the position of the maximum of the Fourier spectrum. The boundary maximum in (a) corresponds to a mean velocity of 7.4 μm/min in the continuous spreading phase. The peak at $s_{\max} = 5$ in (b) corresponds to a repeat time $T = 17 \pm 4$ s for the contractile spreading phase; see Eq. (3). The mean velocity 0.3 μm/min is small. (c) depicts the peak position of the spectrum taken in a running time window with a width of $N = 50$ frames, corresponding to the repeat time T, as a function of the first frame number of the window. Note that the peak position depends on the width of the time window used for Fourier transformation, since frequencies are measured with respect to that width. In (c) we used a smaller window width than in (b), in order to capture the sharpness of the transition.

The transition to the periodic contractile phase is linked to the activity of myosin light chain kinase (MLCK), a protein controlling in turn the activity of myosin motors. Indeed, we found that periodic membrane retractions were absent when inhibiting MLCK [13]. The conjecture is that the actin network contracts or is actively pulled back by myosin motor activity. However, we have no direct evidence yet for the involvement of myosin. Support comes from a theoretical model by Kruse and Jülicher [17], which describes oriented actin fibers connected into a network by molecular motors. They find an instability of homogeneous fiber density towards a contracted state as a function of fiber-motor coupling strength. Moreover, their generic theoretical model allows for oscillatory solutions. Identifying MLCK activity with fiber-motor coupling strength suggests that MLCK could be the control parameter triggering the transition from continuous to periodic contractile spreading. Periodic membrane retractions are a general phenomenon. Indeed, we have found this behavior also in migrating fibroblasts, as well as in endothelial cells. In all these examples, the different phases of spreading result in a spatiotemporal organization of the cytoskeleton capable of sensing substrate stiffness by periodically pulling on the substrate via integrin linkages [13]. Indeed, it is known that cells require stiff substrates for growth and move toward stiffer regions [11,21].

The idea of phases in cell behavior can be applied quite generally. Phases of motility should be considered analogous to the phases of the cell cycle, phases of varying metabolic activity, or different protein expression. We propose to classify cellular behavior in well-defined phases. Their number will be considerably less than an enumeration of concentration and activity levels of all molecular components of the cell. Thus, one can hope to accomplish a simplified description. Moreover, we suggest a hierarchical classification of proteins into modules linked to phase structure, phase regulation parameters, and pure signaling components controlling these parameters. Admittedly, the dividing lines between hierarchy classes are to some extent a matter of definition. However, when all regulatory proteins (and their activities) of a certain cellular subsystem are known, its phase is defined, independent of all the possible states of the signaling network corresponding to this set of parameters. The conceptional advantage of such a classification is that one can completely characterize physical (phase) states of a cell without a complete understanding of the complex signaling network controlling their regulating parameters. Currently, phase classification is not generally done and cellular phenotype cannot be sensibly compared across different genotypes. We expect that some fraction of the variability encountered in biological experiments and the often conflicting results between laboratories stem from the fact that findings corresponding to different cellular phases and boundary conditions are spuriously compared to each other. In conclusion, we feel that the classification of motility into phases can serve as a paradigm for a powerful general ordering principle in quantitative biology.

This work was funded by the Deutsche Forschungsgemeinschaft and the National Institutes of Health via Grant No. GM 036277. H. G. D. would like to thank Adam Meshel and Ana Kostic for helpful discussions.

*Electronic address: hgd@biology.columbia.edu

[1] D. Bray, *Cell Movements: From Molecules to Motility* (Garland Publishing, New York, 2001), 2nd ed.
[2] T. P. Stossel, Science **260**, 1086 (1993).
[3] D. Pantaloni, C. Le Clainche, and M.-F. Carlier, Science **292**, 1502 (2001).
[4] T. D. Pollard and G. G. Borisy, Cell **112**, 453 (2003).
[5] A. Bernheim-Grosswasser, S. Wiesner, R. M. Golsteyn, M.-F Carlier, and C. Sykes, Nature (London) **417**, 308 (2002).
[6] A. Upadhyaya and A. van Oudenaarden, Curr. Biol. **13**, R734 (2003).
[7] F. Gerbal, P. Chaikin, Y. Rabin, and J. Prost, Biophys. J. **79**, 2259 (2000).
[8] M. Dembo and Y.-L. Wang, Biophys. J. **76**, 2307 (1999).
[9] Q. Balaban *et al.*, Nature Cell Biol. **3**, 466 (2001).
[10] G. Jiang, G. Giannone, D. R. Critchley, E. Fukumoto, and M. P. Sheetz, Nature (London) **424**, 334 (2003).
[11] I. B. Bischofs, S. A. Safran, and U. S. Schwarz, Phys. Rev. E **69**, 021911 (2004).
[12] B. Dubin-Thaler, G. Giannone, H.-G. Döbereiner, and M. P. Sheetz, Biophys. J. **86**, 1794 (2004).
[13] G. Giannone, B. Dubin-Thaler, H.-G. Döbereiner, and M. P. Sheetz, Cell **116**, 431 (2004).
[14] R. B. Dickinson and D. L. Purich, Biophys. J. **82**, 605 (2002).
[15] A. Mogilner and G. Oster, Biophys. J. **84**, 1591 (2003).
[16] D. Humphrey, C. Duggan, D. Saha, D. Smith, and J. Käs, Nature (London) **416**, 413 (2002).
[17] K. Kruse and F. Jülicher, Phys. Rev. E **67**, 051913 (2003).
[18] K. Kruse, J. F. Joanny, F. Jülicher, J. Prost, and K. Sekimoto, Phys. Rev. Lett. **92**, 078101 (2004).
[19] H.-G. Döbereiner, E. Evans, M. Kraus, U. Seifert, and M. Wortis, Phys. Rev. E **55**, 4458 (1997).
[20] J. Pécréaux, H.-G. Döbereiner, J. Prost, J.-F. Joanny, and P. Bassereau, Eur. Phys. J. E **13**, 277 (2004).
[21] C. M. Lo, H. B. Wang, M. Dembo, and Y. L. Wang, Biophys. J. **79**, 144 (2000).